ARTICLE NO. 78-1181

Nonlinear Hypersonic Viscous Crossflow Effects on Slender Vehicle Dynamics

Lars E. Ericsson*
Lockheed Missiles and Space Co., Inc., Sunnyvale, Calif.

The laminar boundary layer on the leeside of a slender cone shows a nonlinear high rate of growth prior to separation. It is shown how the mathematical model for the effects on the unsteady aerodynamics is essentially the same as that for the effects of the separation-induced free body vortices at higher angles of attack or of the leading-edge vortices on delta wings. The developed analytic method, which accepts static data as an input, predicts the large dynamic viscous crossflow effects observed in ballistic range tests of a 10-deg slender, sharp cone.

Nomenclature

B = viscous parameter defined in Eq. (1)
c = reference length, $c = d_B$
C^* = Chapman-Rubesin parameter
d = body diameter
k_1, k_0 = parameters defined in Eqs. (4) and (5)
ℓ = sharp cone length
L_F = frustum length
M = Mach number
M_p = pitching moment: coefficient $C_m = M_p/(\rho_\infty U_\infty^2/2)Sc$
N = normal force: coefficient $C_N = N/(\rho_\infty U_\infty^2/2)S$
p = static pressure: coefficient $C_p = (p - p_\infty)/(\rho_\infty U_\infty^2/2)$
Pr = Prandtl number
q = body pitch rate
r = body radius
Re = Reynolds number, $Re_x = xU_e/\nu_e$ and $Re_{x\infty} = xU_\infty/\nu_\infty$
S = reference area, $S = \pi c^2/4$
t = time
T = temperature
T^* = reference temperature
U = axial velocity
$\bar{U}$ = mean convection velocity
x = axial distance from cone apex
z = translatory coordinate
α = angle of attack
$\bar{\alpha}$ = total angle of incidence
α_0 = trim angle of attack
γ = ratio of specific heats ($\gamma = 1.4$ for air)
δ = boundary-layer thickness
δ^* = boundary-layer displacement thickness
Δ = increment
ζ = dimensionless z coordinate, $\zeta = z/c$
θ = body perturbation in pitch
θ_c = cone half angle
ν = kinematic viscosity
ξ = dimensionless x coordinate, $\xi = x/c$
ρ = air density
σ = upwash angle
ϕ = azimuth (Fig. 3)
$\bar{\chi}$ = viscous hypersonic similarity parameter, $\bar{\chi} = M_e^3\sqrt{C^*}/\sqrt{Re_x}$

Subscripts

B = base
c.g. = center of gravity or oscillation center
D = for deformed body portion
e = boundary-layer edge
E = end of leeside "hump"
F = frustum
i = inner layer
ie = inner layer edge
N = nose
R = reference value
t = total or stagnation value
v = viscous effect
w = wall
0 = value at $\alpha = 0$
∞ = freestream value

Superscripts

i = induced, e.g., $\Delta^i C_{Nv}$ = change in normal force due to leeside boundary layer "hump"
$\bar{(\ )}$ = indicates center of pressure, e.g., $\bar{x}_{vi}$ = center of pressure "hump" effect

Derivative Symbols

$\dot{\theta}$ = $\partial\theta/\partial t$
$C_{N\alpha}$ = $dC_N/d\alpha$: $C_{m\theta} = \partial C_m/\partial\theta$
C_{mq} = $\partial C_m/\partial(cq/U_\infty)$: $C_{m\dot{\alpha}} = \partial C_m/\partial(c\dot{\alpha}/U_\infty)$
$C_{m\dot{\theta}}$ = $C_{mq} + C_{m\dot{\alpha}}$

Introduction

IT is well known that viscous interaction effects are important in hypersonic low-density flows. The problem is for the dynamicist to determine from his theoretical and experimental information what the true full-scale flight dynamics will be. Figure 1 illustrates his dilemma. It shows the experimental results compiled by Welsh et al.[1] for a 10-deg sharp cone. Also shown are the inviscid flow results from Brong's theory.[2] The large influence of Mach number is to be expected as the viscous interaction effects increase strongly with increasing Mach number. In Fig. 1 conventional wind tunnel test results and ballistic range data indicate that the viscous effect is slightly destabilizing statically. However, in regard to the dynamic stability, the ballistic range data indicate that the damping increases strongly with increasing Mach number, whereas the wind tunnel results show the

Presented as Paper 78-1181 at the AIAA 11th Fluid and Plasma Dynamics Conference, Seattle, Wash., July 10-12, 1978; submitted July 21, 1978; revision received Feb. 7, 1979.

Index categories: Supersonic and Hypersonic Flow; Boundary Layers and Convective Heat Transfer—Laminar; Nonsteady Aerodynamics.

*Consulting Engineer. Associate Fellow AIAA.

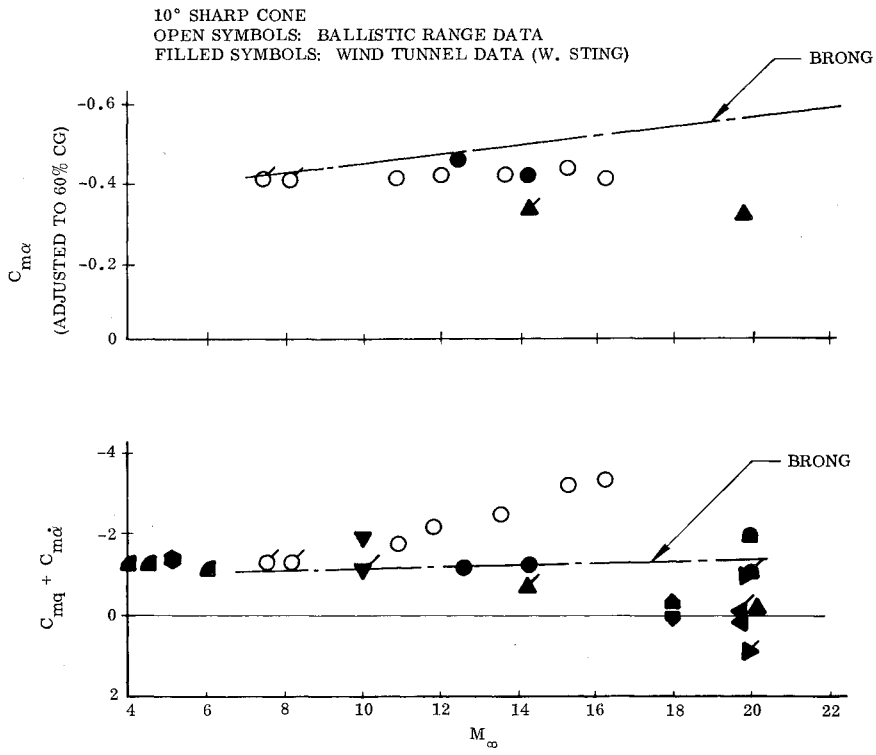

Fig. 1 Unsteady aerodynamic characteristics of 10-deg sharp cones.

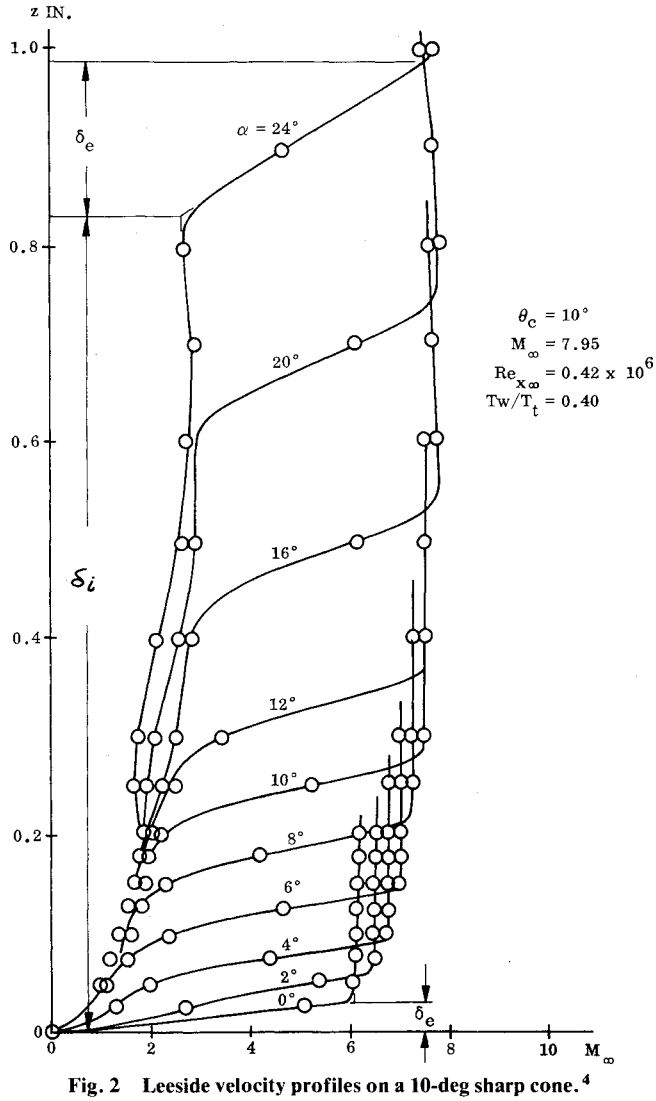

Fig. 2 Leeside velocity profiles on a 10-deg sharp cone.[4]

opposite trend, i.e., a strong reduction of the damping leading to dynamic instability for high Mach numbers. The pertinent information in regard to test conditions, center of gravity, etc., for the test data in Fig. 1 is given in Ref. 3. It is discussed elsewhere[3] how the wind tunnel data can be distorted by dynamic support interference effects. The aim of the present analysis is to demonstrate that the dynamic stability data presented by Welsh et al.[1] show the true viscid-inviscid interation effects, and to develop computational means whereby these dynamic effects can be predicted.

Discussion

The ballistic range data in Fig. 1 displaying the large increase of damping with increasing Mach numbers are for moderately large crossflow angles, $\bar{\alpha} > 2.5$ deg, whereas the rest of the data is for small crossflow angles, $\bar{\alpha} < 2$ deg. It is therefore indicated that the increased damping may be caused by the dynamic effects of large viscous crossflow. Tracy[4] has investigated in great detail the viscous crossflow on a 10-deg cone at $M_\infty = 7.95$. The leeside flow profile (Fig. 2) shows how a low-velocity inner layer of thickness δ_i lifts the shear layer of thickness δ_e high above the surface, as is illustrated in Fig. 3. Figure 4 shows how the shear layer thickness δ_e and the total viscous layer thickness $\delta = \delta_i + \delta_e$ vary with the normalized angle of attack, α/θ_c.

The leeside boundary-layer "hump" (Fig. 3) caused by the inner layer growth (δ_i) will cause a significant pressure increase. The data in Fig. 4 show the slope $d\delta_i/d\alpha$ to be one order of magnitude larger than $d\delta_e/d\alpha$ for angles of attack $\alpha/\theta_c > 0.2$. That is, even when the regular viscisd-inviscid interaction effects at low angles of attack, α/θ_c, are negligibly small, this viscous effect at high crossflows can be large.

Figure 2 shows the inner layer to have a much fuller profile than the laminar outer shear layer. Considering the crossflow-induced increased mixing, this is not too surprising. The present analysis will deal mainly with the characteristics of this leeward side nonlinear "hump" generated by forward crossflow effects. The linear local crossflow effects first described by Moore[5] and later extended to unsteady flow by Orlik-Rückemann[6] will not be considered. They have a negligible influence on the stability derivatives of a cone when

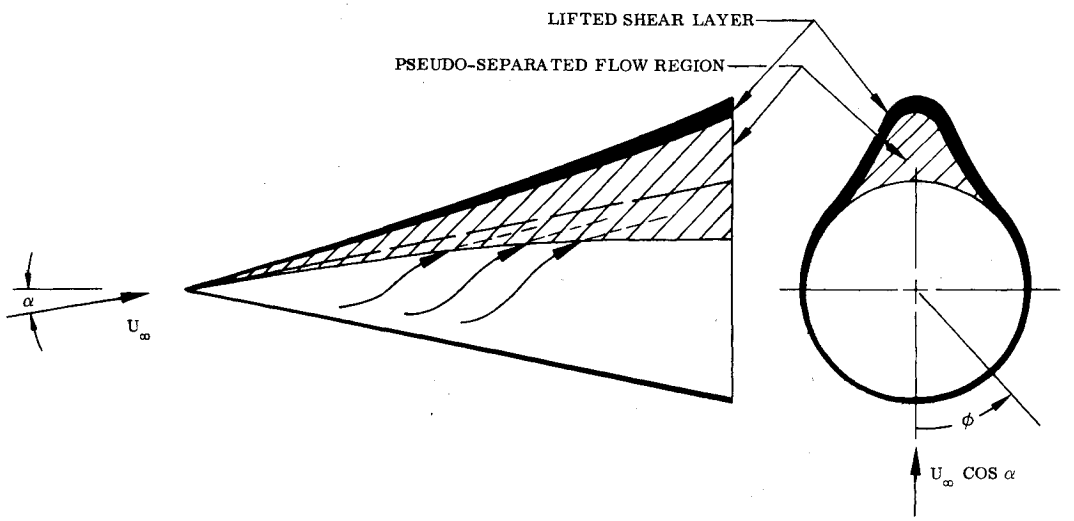

Fig. 3 Conceptual viscous crossflow on a sharp cone.

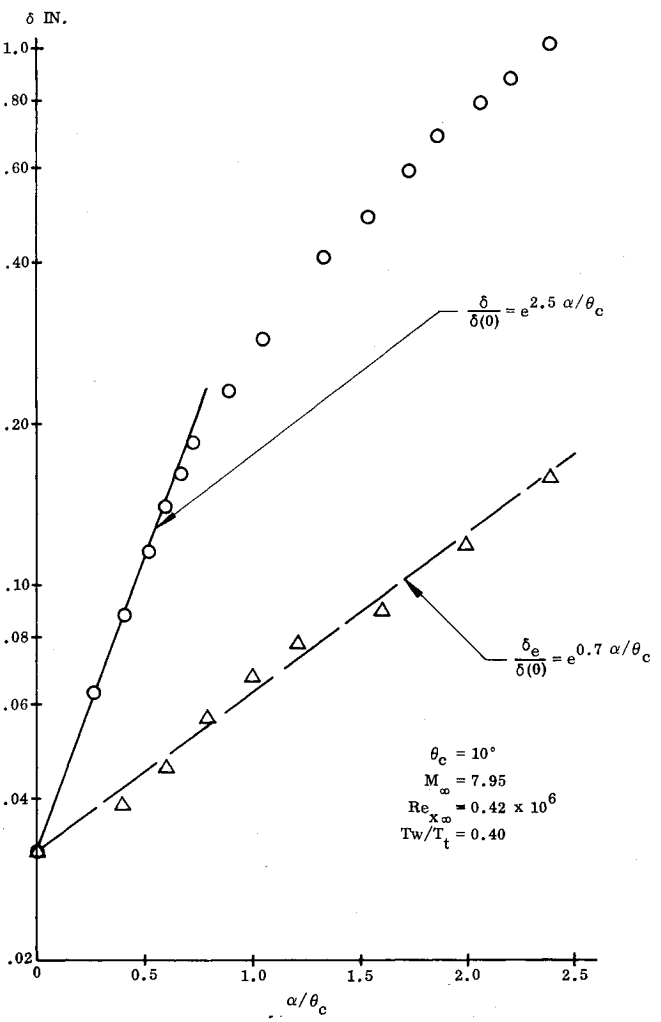

Fig. 4 Measured shear layer thickness on the top meridian of a 10-deg sharp cone.[4]

either the c.g. is close to 60% (of sharp cone length) or the angle of attack is large. Thus, they cannot explain the trend of the ballistic range data in Fig. 1.

Analysis

The boundary-layer growth on slender cones will be analyzed first, and simple analytic approximations will then be sought for the static and dynamic viscid-inviscid interactions.

Boundary-Layer Growth

The boundary-layer displacement surface will increase the inviscid flow deflection angle and cause a corresponding pressure increase. The Mangler-transformed laminar boundary-layer equations for a cone give[7-10]

$$\frac{\delta^*}{x} = \frac{2B}{\sqrt{3}} \frac{M_e^2\sqrt{C^*}}{\sqrt{Re_x}} \tag{1a}$$

$$Pr=0.725;\ B=0.1445(\gamma-1)+\left(0.9685\frac{T_w}{T_e}-0.1035\right)\Big/M_e^2$$

$$=(\gamma-1)\left(0.1445+0.4843\frac{T_w}{T_t}\right)+\left(0.9685\frac{T_w}{T_t}-0.1035\right)\Big/M_e^2 \tag{1b}$$

$$Pr=1;\ B=0.166(\gamma-1)+0.865\frac{T_w}{T_e}\Big/M_e^2$$

$$=(\gamma-1)\left(0.166+0.4325\frac{T_w}{T_t}\right)+0.865\frac{T_w}{T_t}\Big/M_e^2 \tag{1c}$$

According to Ref. 11, $C^*=1$ for $T^*\leq 200°$R and

$$C^*=\frac{T^*}{T_t}\left(1+\frac{\gamma-1}{2}M_e^2\right)^{-0.24}$$

for reference temperatures in the range $200°\text{F} < T^* < 1000°$R, where $T^*/T_t = (1+3T_w/T_t)/6$.

It can be shown[9] that the ratio δ/δ^* is simply

$$\delta/\delta^* = 1+2/BM_e^2 \tag{2}$$

At hypersonic speeds, $M_e^2 \gg 1$, B varies negligibly with Mach number. Thus, B is constant for constant T_w/T_e. Equations (1) and (2) together define how the laminar boundary-layer thickness changes due to changing ambient conditions at the boundary-layer edge.

$$\frac{\delta_e(\alpha)}{\delta_e(0)} = \frac{1+[2/BM_e^2(\alpha)]}{1+[2/BM_e^2(0)]}\frac{M_e^2(\alpha)}{M_e^2(0)}\Big/\sqrt{\frac{Re_x(\alpha)}{Re_x(0)}} \tag{3}$$

In addition to the change of boundary-layer thickness with angle of attack described by Eq. (3) the thickness also changes due to local viscous crossflow.[5,6] However, for the lifted layer on the leeward side (Figs. 3 and 4), these local viscous crossflow effects are probably negligible. For the case $\alpha=\theta_c$ the inviscid flow parameters on the top leeward meridian,

$\phi = \pi$, are equal to the freestream values according to Newtonian theory, which in Eq. (3) gives $\delta_e(\alpha)/\delta_e(0) = 2.04$ for $\alpha = \theta_c = 10$ deg. This is in good agreement with the experimental result in Fig. 4, which is $\delta_e/\delta(0) = e^{0.7} = 2.01$. This tends to confirm that the (local) crossflow effects on the outer lifted layer are negligible.

Equation (1) represents the boundary-layer growth with x at a constant angle of attack, as affected by the tangent cone edge condition at that angle of attack. However, at angle of attack the leeside boundary-layer growth is due largely to mass addition through viscous crossflow. Using local linearization, one can assume that for small perturbations the local boundary-layer thickness will increase linearly with the change of local angle of attack. Thus, the inner layer growth is expressed as follows:

$$\Delta\delta_i^* = k_I \Delta\alpha \tag{4}$$

As in the case of local crossflow effects[5] the thickness change with angle of attack is proportional to the hypersonic similarity parameter $M_\infty \theta_c$. Thus, in a first approximation one would assume that k_I can be expressed as follows

$$k_I = k_0 M_\infty \theta_c \delta_{eR}^* \tag{5}$$

where δ_{eR}^* is a reference shear layer thickness at a certain location used to obtain the local value of k_0. Until more information becomes available in regard to k_I, it will be approximated by Eq. (5) assuming $T_w = T_e$ when determining δ_{er}^*. k_0 is a constant for constant azimuth (ϕ) but will vary with angle of attack. However, in the locally linearized representation of Eq. (5) k_0 is assumed constant for small perturbations ($\Delta\alpha/\theta_c$). According to the results of Ref. 12, one would expect k_0 to be relatively independent of Mach number at hypersonic speeds.

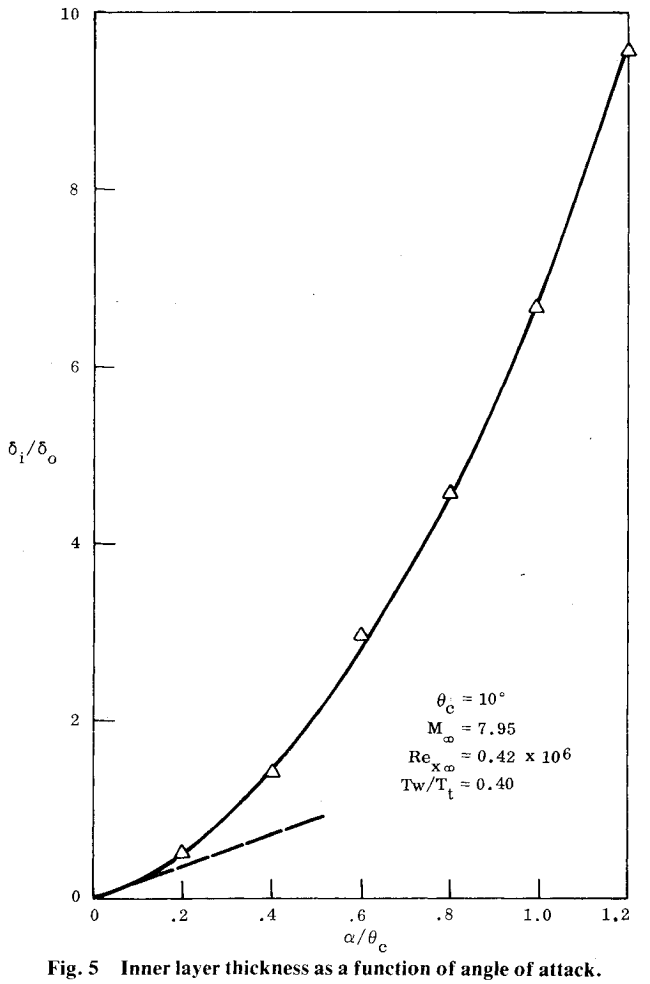

Fig. 5 Inner layer thickness as a function of angle of attack.

δ_i/δ_0, extracted from Tracy's data[4] in Fig. 4, is shown in Fig. 5. The results show the expected nonlinear dependence on α/θ_c of the inner layer thickness. The initial slope, $\partial(\delta_i/\delta_0)/\partial(\alpha/\theta_c) = 2.5 - 0.7 = 1.8$, shown by the dashed line in Fig. 5, is according to Tracy[4] in good agreement with the local linear crossflow effect predicted by Moore.[5] This local crossflow effect is, however, decreasing with angle of attack and is probably negligible at $\alpha/\theta_c > 0.5$.

In order to determine how much of the increase in inner layer displacement thickness between $\alpha/\theta_c = 0$ and 1.0 is caused by mass addition to the leeside "hump," the k_I effect, one needs to know the boundary conditions at the edge of the inner layer. It was shown earlier that the lifted layer behaved as if the inner layer had been the wall. Thus, in agreement with the earlier assumption $T_w = T_e$ one obtains $T_w = T_{ie} = T_e$. Thus,

$$U_{ie}/U_e = M_{ie}/M_e \tag{6}$$

The experimental results[4] show $M_{ie}/M_e \approx 0.28$ for $\alpha/\theta_c \leq 1.0$. It is shown in the Appendix of Ref. 13 how the experimental data from the tests by Tracy[4] and by Stetson et al.[14] can be used to define the following aerodynamic derivatives for the leeside "hump" effect:

$$\Delta^i C_{N\alpha v} = -0.312\left(\frac{x_E}{L_F}\right)\left(1 - \frac{r_N}{r_B}\right)^2 \frac{\partial[\Delta^i C_p(\pi)/2\theta_c^2]}{\partial(\alpha/\theta_c)} \tag{7a}$$

$$\Delta^i C_{m\alpha v} = -\frac{\Delta^i C_{N\alpha v}}{2\theta_c}\left(1 - \frac{r_N}{r_B}\right)\left(\frac{\bar{x}_{iv}}{L_F} - \frac{x_{c.g.}}{L_F}\right) \tag{7b}$$

$$\frac{\bar{x}_{iv}}{L_F} = \frac{r_N}{r_B} + 0.70\left(1 - \frac{r_N}{r_B}\right)\frac{x_E}{L_F} \tag{7c}$$

Unsteady Aerodynamics

It has been shown in the previous sections that the pressure increase due to crossflow effects on the "viscous hump" is determined by $\Delta\delta_i^*$, as given by Eq. (4). The thickness $\Delta\delta_i^*$ at any location ξ is the integral result of the mass addition to the "hump" from all stations on the body upstream of ξ. This gives a complete analogy to the vortex-induced pressure changes on a delta wing.[15] Consequently, the analytic method developed in Ref. 15 can be applied here when formulating the contribution of $\Delta^i C_{pv}$ to the slender cone unsteady aerodynamics.

It was demonstrated in Ref. 15 that the quasisteady equivalent to a pitching body is a stationary deformed (bent) body. $\Delta\delta_i^*$ at any downstream station is given by the integral over the deformed body upstream of this station. That is, $\Delta\delta_i^*$ at ξ is determined as follows, using Eq. (4):

$$\Delta\delta_i^* = k_I \int_D \Delta\alpha \, d\xi \tag{8}$$

The angle of attack change due to body deformation is

$$\Delta\alpha = \frac{\partial z}{dx} = \frac{\partial \zeta}{\partial \xi} \tag{9}$$

Thus, Eq. (8) gives simply

$$\Delta\delta_i^* = k_I \Delta\zeta_D \tag{10}$$

where $\Delta\zeta_D$ is the total translatory displacement (measured in reference lengths, $\Delta\zeta_D = \Delta z_D/c$) due to body deformation, $\Delta\zeta_D = \zeta(\xi) - \zeta(0)$. That is, the incremental thickness $\Delta\delta_i^*$ at station ξ is proportional to the translatory deflection relative

to cone apex independently of how this total deflection is composed ($\Delta\delta_I^*$ is independent of the bending mode shape).

In the unsteady case the local effective perturbation angle due to the deformation is

$$\Delta\tilde{\alpha}(\xi) = \frac{\partial\zeta}{\partial\xi} + \frac{c}{U_\infty}\frac{\partial\zeta}{\partial t} \tag{11}$$

At station ξ_I, at time t_I, the incremental slope is the result of the total perturbation-induced contributions to the inner layer thickness from each station ξ upstream of ξ_I at the earlier time $t_I - c(\xi - \xi_I)/\bar{U}$, where $\bar{U}$ is the mean convection velocity in the inner layer. As in the steady case the incremental slope is determined by the deflection relative to that at the apex (at time $t - c\xi_I/\bar{U}$) indpendently of the deflection mode shape. Thus, the thickness increment at station ξ can be written

$$\Delta\delta_I^*(\xi,t) = k_I[\zeta(\xi,t) - \zeta\{0, t-(c\xi/\bar{U})\}] \tag{12}$$

For rigid body oscillations in pitch (θ) around c.g. at $\alpha = \alpha_0$, one can write the deflection ζ as follows for small amplitudes $|\theta|$

$$\zeta = \zeta_{c.g.} + (\xi - \xi_{c.g.})\theta \tag{13}$$

and Eq. (12) becomes

$$\Delta\delta_I^*(\xi,t) = k_I[(\xi - \xi_{c.g.})\theta(t) + \xi_{c.g.}\theta\{t-(c\xi/\bar{U})\}] \tag{14}$$

For the low reduced frequencies and moderate amplitudes of interest, $\bar{\omega}^2 \ll 1$ and $(\bar{\omega}\Delta\theta)^2 \ll 1$, one can express $\theta(t - c\xi/\bar{U})$ in form of a Taylor expansion

$$\theta\left(t - \frac{c\xi}{\bar{U}}\right) = \theta(t) - \frac{c\xi}{\bar{U}}\dot{\theta}(t)\ldots \tag{15}$$

Thus, Eq. (14) becomes

$$\Delta\delta_I^*(\xi,t) = k_I\xi\left[\theta(t) - \xi_{c.g.}\frac{U_\infty}{\bar{U}}\frac{c\dot{\theta}(t)}{U_\infty}\right] \tag{16}$$

In the static case $\Delta\zeta_D$ in Eq. (10) is for the rigid body

$$\Delta\zeta_D = \xi\theta \tag{17}$$

The analysis in the Appendix of Ref. 13 gives

$$\frac{\partial}{\partial\theta}\left(\frac{d\Delta^i C_{Nv}}{d\xi}\right) \sim \frac{\partial}{\partial\theta}(\Delta\delta_I^*) \tag{18a}$$

$$\frac{\partial}{\partial(c\dot{\theta}/U_\infty)}\left(\frac{d\Delta^i C_{Nv}}{d\xi}\right) \sim \frac{\partial}{\partial(c\dot{\theta}/U_\infty)}(\Delta\delta_I^*) \tag{18b}$$

That is, the induced force derivatives are proportional to the corresponding rates of change of the viscous "hump."

Combining Eqs. (16) and (18) one obtains the following simple formulation for the contribution of the "viscous hump" to the damping in pitch

$$\frac{\partial}{\partial(c\dot{\theta}/U_\infty)}\left(\frac{d\Delta^i C_{Nv}}{d\xi}\right) = -\xi_{c.g.}\frac{U_\infty}{\bar{U}}\frac{\partial}{\partial\theta}\left(\frac{d\Delta^i C_{Nv}}{d\xi}\right) \tag{19}$$

This leads to the following simple result for the contributions to the stability derivatives

$$\Delta^i C_{m\dot{\theta}v} = -\xi_{c.g.}\frac{U_\infty}{\bar{U}}\Delta^i C_{m\theta v} \tag{20}$$

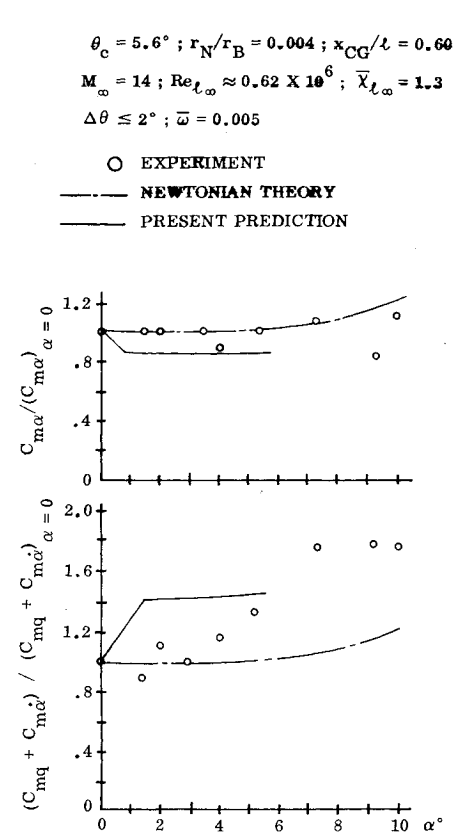

Fig. 6 Nonlinear viscous effects on sharp cone unsteady aerodynamics.

where $\Delta^i C_{m\theta v} = \Delta^i C_{m\alpha v}$. Equation (20) reveals that the large viscous crossflow will affect static and dynamic stability in opposite ways.

In a hypersonic turbulent boundary layer the convection velocity $\bar{U}$ varies from $\bar{U}/U = 0.6$ near the wall to $\bar{U}/U = 0.8$ in the outer layer.[16,17] For lack of a better estimate, it will be assumed that the mean convection velocity in the inner pseudoseparated flow region is represented by $\bar{U}_{ie}/U_{ie} = 0.6$. Thus, the mean convection velocity $\bar{U}_{ie}$ is obtained as follows[18]:

$$\frac{\bar{U}_{ie}}{U_\infty} = 0.6\frac{U_{ie}}{U_e}\frac{U_e}{U_\infty} \tag{21a}$$

$$\frac{U_e}{U_\infty} = \frac{M_e}{M_\infty}\left\{\frac{1+[(\gamma-1)/2]M_\infty^2}{1+[(\gamma-1)/2]M_e^2}\right\}^{1/2} \tag{21b}$$

$U_{ie}/U_e = M_{ie}/M_e$ according to Eq. (6) where $M_{ie}/M_e = 0.28$ for Tracy's test condition.[4]

McDevitt and Mellenthin[19] in their test of a 10-deg cone at $M_\infty = 7.40$ measured upwash angles σ that gave the following ratio between outer and inner layer flow conditions: $0.3 < \sigma_e/\sigma_{ie} < 0.4$. Considering that $\bar{U}_{ie}/U_e < \sigma_e/\sigma_{ie}$ one finds this to be in basic agreement with the ratio 0.28 indicated earlier for Tracy's test. Considering further that $M_{ie}/M_e \approx 0.28$ for $0 \leq \alpha/\theta_c \leq 1.0$ regardless of the large changes of shear layer thickness over this angle-of-attack range (Fig. 2) one feels justified to assume that the flow profiles are similar for hypersonic flow conditions. Consequently, it will be assumed that $U_{ie}/U_e \approx 0.28$ giving

$$\bar{U}_{ie}/U_e \approx 0.17 \tag{22}$$

The only dynamic test data known by the present author to be detailed enough to illustrate the dynamic viscid-inviscid interaction discussed in this paper are those obtained by

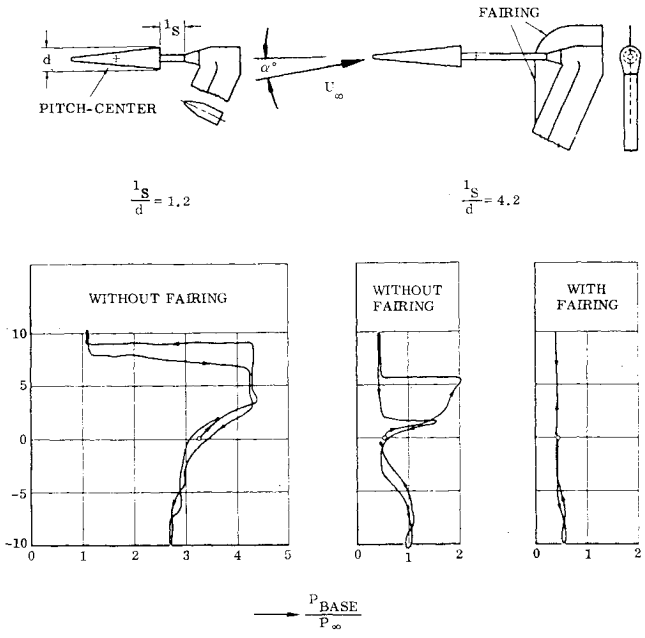

Fig. 7 Sting support effects on base pressure.[20]

Walchner and Clay[20] for the same 5.6-deg cone tested by Stetson[14] in the same test facility. The only difference is that the Reynolds number in the dynamic test was 30% lower than in the static test. Consequently $\Delta^i C_{pv}(\pi)/2\theta_c^2$ from Stetson's test[14] is increased by 15%.

With $x_E/\ell \approx 1.0$ (flat base) and $r_N/r_B = 0$ (sharp cone) Eq. (7) gives the following moment derivative for $x_{c.g.}/\ell = 0.60$ and $\theta_c = 5.6$ deg:

$$\Delta^i C_{m\alpha v} = 0.160\partial\left[\frac{\Delta^i C_{pv}(\pi)}{2\theta_c^2}\right]\Big/\partial\left(\frac{\alpha}{\theta_c}\right) \tag{23}$$

For slender cones $U_e \approx U_\infty$ and Eqs. (20-22) give

$$\Delta^i C_{m\dot{\theta}v} = -18\Delta^i C_{m\alpha v} \tag{24}$$

The result in Eq. (24) illustrates an important character of this "viscous hump" effect, i.e., the effect on slender vehicle dynamics is one order of magnitude larger than the effect on static stability. In order to assess the relative importance of these viscous contributions one needs to know the inviscid flow stability derivatives. They can be obtained simply by the methods of Ref. 21.

For a sharp slender cone (with $\tan\theta_c = \theta_c$) at $\alpha = 0$ Newtonian theory gives

$$C_{m\alpha} = -\frac{1}{\theta_c}\left(\frac{2}{3} - \frac{x_{c.g.}}{\ell} + \theta_c^2\right) \tag{25a}$$

$$C_{mq} = -\frac{1}{4\theta_c^2}\left[\left(1 + \theta_c^2 - \frac{4}{3}\frac{x_{c.g.}}{\ell}\right)^2 + \frac{2}{9}\left(\frac{x_{c.g.}}{\ell}\right)^2\right] \tag{25b}$$

Using Eqs. (23-25) together with Stetson's data (increased by 15%) gives the prediction shown in Fig. 6.† There is an apparent α-zero shift between experimental data and prediction. Figure 7 shows the asymmetric sting support system used in the test.[20] Without the sting-strut fairing, the base pressure shows asymmetric support interference even for the long sting, which gave the correct damping data at $\alpha = 0$. One notes in Fig. 7 that the base pressure at $\alpha = 0$ is closely the same as with the fairing on. Thus, it is to be expected that some sting interference effects are present in the measurements at $\alpha > 0$ in Fig. 6. The sting-strut blockage will obstruct the downwash from the cone at $\alpha > 0$, thus causing an α-zero shift and probably also changing the magnitude of the measured stability derivatives.

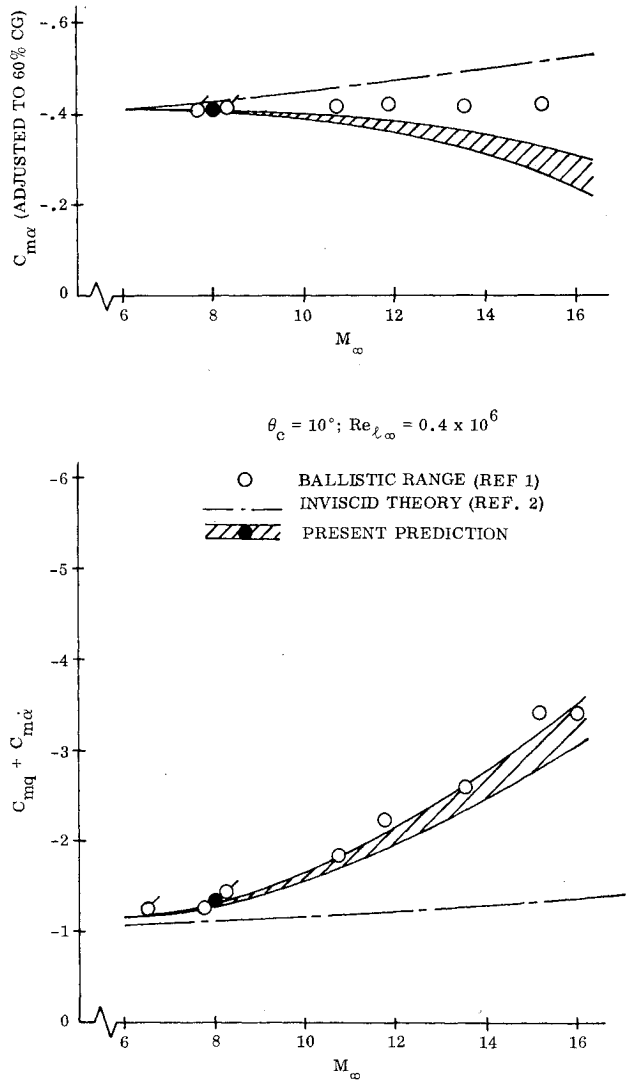

Fig. 8 Comparison between predicted and measured unsteady aerodynamics of a 10-deg cone.

The 10-deg cone tested in the ballistic range by Welsh et al.[1] at $Re_{\ell\infty} = 0.4 \times 10^6$ has a $\bar{\chi}_R$ value that is 32% higher than for Tracy's test (at the same Mach number). Consequently, the pressure generated by the viscous "hump" is 32% higher than in Tracy's test. Neglecting the small amount of nose bluntness present in the ballistic range test,‡ Eq. (7) gives (for $x_{c.g.}/\ell = 0.63$ and $\theta_c = 10$ deg)

$$\Delta^i C_{m\alpha v} = 0.063\partial\left[\frac{\Delta^i C_p(\pi)}{2\theta_c^2}\right]\Big/\partial\left(\frac{\alpha}{\theta_c}\right) \le 0.0187 \tag{26}$$

With $U_e/U_\infty \approx 1$, Eqs. (20) and (22) give

$$\Delta^i C_{m\dot{\theta}v} = -10.7\Delta^i C_{m\alpha v} \ge -0.20 \tag{27}$$

The result for 60% c.g. is

$$\Delta^i C_{m\alpha v} = 0.090\partial\left[\frac{\Delta^i C_p(\pi)}{2\theta_c^2}\right]\Big/\partial\left(\frac{\partial}{\theta_c}\right) \le 0.0267 \tag{28}$$

†Equation (25) has been modified according to Ref. 21 to include the weak nonlinear effect of α for the Newtonian prediction in Fig. 6.

‡Welsh et al. have in later tests found that the blunting during the runs is negligible, i.e., $d_N/d_B = 0.032$.

According to the analysis in the Appendix of Ref. 13 for $0.2 \leq \alpha/\theta_c \leq 1.0$ one should be able to use $\chi_R \approx \chi_\infty$ giving the following expression for extrapolation of Mach number effects:

$$\frac{(\Delta^i C_{m\alpha v})_1}{(\Delta^i C_{m\alpha v})_2} = \frac{(\Delta^i C_{m\dot{\theta} v})_1}{(\Delta^i C_{m\dot{\theta} v})_2} = \frac{(M_\infty^3)_1}{(M_\infty^3)_2} \tag{29}$$

Combining Eqs. (26-29) one obtains the prediction shown in Fig. 8. It is assumed that $\alpha_{\text{effective}} > 0.25\ \theta_c$ and the extrapolation is made from the solid data point at $M_\infty = 7.95$. The computed viscous effect was added in one case to the inviscid theory at Brong, in the other case to the Newtonian value, giving the spread in prediction indicted by the cross-hatched region.

It can be seen that there is good agreement between prediction and experiment of the dynamic but not for the static stability derivative. The reason for this is not clear at the present time. However, it should be noted that the static data were transferred to 60% c.g. and that the deviation between the inviscid theory and viscous experimental results is much less in regard to static than in regard to dynamic stability. This leaves more room for errors in evaluating the viscous effect on the static stability derivative. The local crossflow effects with the load center at 60% will be statically stabilizing for c.g. aft of 60%. This is demonstrated by recent results published by Adams et al.[22] With c.g. at 67.7% the local crossflow effects dominated in his case over the "hump" effect. It was shown that these statically stabilizing local crossflow effects had disappeared at $\alpha/\theta_c > 0.5$ in agreement with present results for $\phi = 140$ deg (see Appendix of Ref. 13). A more complete comparison with the results in Ref. 22 will be made some time in the future when the methods of Ref. 23 have been extended to apply to the sharp cone.

To the best of the author's knowledge the experimental dynamic results in Refs. 1 and 20 are the only ones available for which the present analysis could be performed. In regard to dynamic wind-tunnel experiments, one has the problem of support interference and the difficulty of determining the aerodynamic spring $C_{m\alpha}$ with sufficient accuracy. Awaiting the appearance of a new independent set of data against which the present analysis can be tested the following can be said in regard to its validity.

The present analysis gives a uniform mathematical representation of the effects of nonlinear viscous crossflow on slender vehicle dynamics. The mechanics of the boundary-layer crossflow feeding to the leeside of a slender cone do not change when the flow starts to separate. Furthermore, the mechanics remain the same when the cross section is gradually changed from circular via elliptic to that representative of a slender delta wing. Such similarity has also been observed by others.[24,25] Finally, the mathematical relationship between dynamic and static nonlinear viscous crossflow effects remains the same throughout the speed region from incompressible to hypersonic Mach numbers. This is in agreement with the general observation made by Wang[26] in regard to separated flow vortices. However, the static aerodynamic characteristics induced by the nonlinear viscous crossflow do themselves change greatly with geometry and test environment. Further analysis using both numerical results, of the type discussed in Ref. 22, and experimental data, if possible more detailed than those used here,[4,14] should lead to the formulation of a simple analytic theory through which the nonlinear viscous crossflow effects of unsteady aerodynamics can be predicted ("from scratch") with sufficient accuracy for preliminary design.

Conclusions

The analysis of viscous crossflow effects on hypersonic unsteady aerodynamics of slender cones has shown the following:

1) The effect of large viscous crossflow can be significant even when the viscid-inviscid interaction at small angles of attack is negligibly small.

2) Large viscous crossflow affects static and dynamic stability in opposite ways, e.g., decreasing static and increasing dynamic stability of statically stable vehicles. The crossflow effects increase with Mach number as M_∞^3 for constant Reynolds number ($Re_{l\infty}$).

3) The developed analytic methods can predict the unsteady aerodynamic characteristics of large viscous crossflow if the static characteristics are known. Using static experimental characteristics gives predictions that are in good agreement with experimental dynamic data.

4) The effects of large viscous crossflow on vehicle dynamics of slender cones are in many aspects similar to the effects of boundary-layer transition. Thus, the effect on dynamic characteristics is one order of magnitude larger than the effect on static characteristics.

The large viscous crossflow phenomenon discussed in the present paper could have important impact on pitch-yaw-roll coupling of slender re-entry vehicles, effects that will be highly amplified for ablating vehicles. The pretransition behavior observed in Earth re-entry may well be caused by the effects of large viscous crossflow.

References

[1] Welsch, C. J., Winchenbach, G. L., and Madagan, A. N., "Free-Flight Investigation of the Aerodynamic Characteristics of a Cone at High Mach Numbers," *AIAA Journal*, Vol. 8, Feb. 1970, pp. 294-300.

[2] Brong, E. A., "The Unsteady Flow Field about a Right Circular Cone in Unsteady Flight," FDL-TDR-64-148, Air Force Flight Dynamics Laboratory, Jan. 1967.

[3] Ericsson, L. E. and Reding, J. P., "Viscous Interaction or Support Interference?—The Dynamicist's Dilemma," *AIAA Journal*, Vol. 16, April 1978, pp. 363-368.

[4] Tracy, R. C., "Hypersonic Flow over a Yawed Circular Cone," California Institute of Technology, Pasadena, Calif., CIT/GAL Memo. No. 69, Aug. 1963.

[5] Moore, F. K., "Laminar Boundary Layer on a Circular Cone in Supersonic Flow at a Small Angle of Attack," NACA TN 2521, Oct. 1951.

[6] Orlik-Rückemann, K. J., "Dynamic Viscous Pressure Interaction in Hypersonic Flow," National Research Council of Canada, NRC, NAE Aero Rept. LR-535, July 1970.

[7] Hayes, W. D. and Probstein, R. F., *Hypersonic Flow Theory*, Academic Press, New York and London, 1959, pp. 341-353.

[8] Ericsson, L. E., Almroth, B. O., Bailie, J. A., Brogan, F. A., and Stanley, G. M., "Hypersonic Aeroelastic Analysis," Lockheed Missiles and Space Co., Sunnyvale, Calif., LMSC-D056746, Contract N62269-73C-0713, Sept. 1975.

[9] Eckstrom, D. J., "Engineeering Analysis of Boundary Layers and Skin Friction on Bodies of Revolution at Zero Angle of Attack," Lockheed Missiles and Space Co., Sunnyvale, Calif., LMSC/805162, TM 55-21-21, May 1965.

[10] Schlichting, H., *Boundary Layer Theory*, translated by J. Kestin, McGraw-Hill Book Co., London, 1955.

[11] Sliski, N. J., "An Analytical and Experimental Investigation of Hypersonic Interaction Pressure Effects," Air Force Flight Dynamics Laboratory, Wright-Patterson Air Force Base, Ohio, AFFDL-TR-73-58, Nov. 1973.

[12] Ericsson, L. E., "Correlation of Attitude Effects on Slender Vehicle Transition," *AIAA Journal*, Vol. 12, April 1974, pp. 523-529.

[13] Ericsson, L. E., "Nonlinear Hypersonic Viscous Crossflow Effects on Slender Vehicle Dynamics," AIAA Paper 78-1181, Seattle, Wash., July 1978.

[14] Stetson, K. F., "Boundary-Layer Separation on Slender Cones at Angle of Attack," *AIAA Journal*, Vol. 10, May 1972, pp. 642-648.

[15] Ericsson, L. E. and Reding, J. P., "Unsteady Aerodynamics of Slender Delta Wings at Large Angles of Attack," *Journal of Aircraft*, Vol. 12, Sept. 1975, pp. 721-729.

[16] Kistler, A. L. and Chen, W. S., "The Fluctuating Pressure Field in a Supersonic Turbulent Boundary Layer," California Institute of Technology, Pasadena, Calif., JPL TR-32-277, Aug. 1972.

[17] Owen, F. K. and Horstman, C. C., "A Study of Turbulence Generation in a Hypersonic Boundary Layer," AIAA Paper 72-182, San Diego, Calif., June 1972.

[18] Ames Research Staff, "Equations, Tables, and Charts for Compressible Flow," NACA Rept. 1135, 1953.

[19] McDevitt, J. B. and Mellenthin, J. A., "Upwash Patterns on Ablating and Nonablating Cones at Hypersonic Speeds," NASA TN D-6203, March 1971.

[20] Walchner, O. and Clay, J. T., "Nose Bluntness Effects on the Stability Derivatives of Cones in Hypersonic Flow," *Transactions of the Second Technical Workshop on Dynamic Stability Testing*, Paper 8, Vol. 1, April 1965.

[21] Ericsson, L. E., "Unsteady Embedded Newtonian Flow," *Astronautica Acta*, Vol. 18, Nov. 1973, pp. 309-330.

[22] Adams, J. C., Jr. and Griffith, B. J., "Hypersonic Viscous Static Stability of a Sharp 5-Deg Cone at Incidence," *AIAA Journal*, Vol. 14, Aug. 1976, pp. 1062-1068.

[23] Ericsson, L. E., "Viscous and Elastic Perturbation Effects on Hypersonic Unsteady Airfoil Aerodynamics," *AIAA Journal*, Vol. 15, Sept. 1977, pp. 1481-1490.

[24] Whitehead, A. H., Jr., Hefner, J. N., and Rau, D. M., "Lee Surface Vortex Effects Over Configurations in Hypersonic Flow," AIAA Paper 72-77, San Diego, Calif., Jan. 1972.

[25] Dunavant, J. C., Mayaran, K. Y., and Wahlbert, G. D., "A Survey of Leeside Flows and Heat Transfer on Delta Planform Configurations," AIAA Paper 76-118, Washington, D.C., Jan. 1976.

[26] Wang, K. C., "Separation of Three-Dimensional Flow," Martin Marietta Lab., Baltimore, Md., MML TR-76-54C, Aug. 1976.